




Empirical Atomic Data for Plasma Simulations

Stephan Fritzsche^{1,2,3,*} , Houke Huang^{1,2}  and Aloka Kumar Sahoo^{1,2} 

- ¹ Helmholtz-Institut Jena, Fröbelstieg 3, D-07743 Jena, Germany; huanghouke@impcas.ac.cn (H.H.); a.k.sahoo@hi-jena.gsi.de (A.K.S.)
² GSI Helmholtzzentrum für Schwerionenforschung, D-64291 Darmstadt, Germany
³ Theoretisch-Physikalisches Institut, Friedrich-Schiller-Universität Jena, D-07743 Jena, Germany
* Correspondence: s.fritzsche@gsi.de

Abstract

Recent advances in non-local thermodynamic equilibrium (non-LTE) plasma simulations, for example in modeling kilonova ejecta, have emphasized the need for consistent and reliable atomic data. Unlike LTE modeling, non-LTE calculations must include a consistent treatment of various photon-induced and collisional processes in order to describe realistic electron and photon distributions in the plasma. However, the available atomic data are often incomplete, inconsistently formatted, or even fail to indicate the main dependencies on the level structure and plasma parameters, thus limiting their practical use. To address these issues, we have extended JAC, the Jena Atomic Calculator (version v0.3.0), to provide direct access to relevant cross sections, plasma rates, and rate coefficients. Emphasis is placed on photoexcitation and ionization processes as well as their time-reversed counterparts—photo-de-excitation and photorecombination. Whereas most of these data are still based on empirical expressions, their dependence on the ionic level structure and plasma temperature is made explicit here. Moreover, the electron and photon distributions can be readily controlled and adjusted by the user. This transparent representation of atomic data for photon-mediated processes, together with a straightforward use, facilitates their integration into existing plasma codes and improves the interpretation of high-energy astrophysical phenomena. It may support also more accurate and flexible non-LTE plasma simulations.

Keywords: atomic data; atomic processes in plasma; atoms and ions; collisional excitation; Jena Atomic Calculator; non-LTE plasma simulations; photoexcitation and photo-de-excitation; photoionization and photorecombination; plasma rates and rate coefficients; relativistic



Academic Editor: Andrey Starikovskiy

Received: 15 December 2025

Revised: 21 December 2025

Accepted: 23 December 2025

Published: 29 December 2025

Copyright: © 2025 by the authors. Licensee MDPI, Basel, Switzerland. This article is an open access article distributed under the terms and conditions of the [Creative Commons Attribution \(CC BY\) license](https://creativecommons.org/licenses/by/4.0/).

1. Introduction

Non-local thermodynamic equilibrium (non-LTE) plasma simulations have attracted recent interest in astrophysics and plasma physics [1–3]. The previously assumed LTE often fails for systems such as kilonova ejecta, supernova remnants, stellar atmospheres, fusion plasmas, and warm dense matter, to recall just a few. These systems are usually characterized by steep gradients in temperature or density and strong radiation fields. Contemporary particle-in-cell and radiation-transport codes therefore require extensive and internally consistent datasets [4–6], which include plasma rates and rate coefficients of various collisional and photon-induced processes. Presently, however, existing datasets are often incomplete or inconsistent, and may hence severely limit the predictive power of non-LTE plasma models [7–9].

Indeed, the inconsistent presentation and availability of atomic data pose a major obstacle for present-day non-LTE plasma modeling. Cross sections, plasma rates, and rate coefficients were often published in non-standard or even inconsistent physical units, making dimensional analysis difficult or impossible. Moreover, the physical notation of these data varies between sources in the literature and seldom conveys the assumptions or approximations that were used in deriving them. Several of the employed empirical approximations were originally developed for limited parameter ranges but are meanwhile applied far beyond their initial scope [10,11]. In practice, overcoming these limitations appears to be quite difficult. A keystone to address these issues is the adoption of a consistent and physically meaningful notation. We here—attempt to—provide such a notation for photoionization and photorecombination processes in order to clearly distinguish between alternative empirical formulations and their underlying assumptions. We also demonstrate how this notation can be implemented into JAC, the Jena Atomic Calculator [12,13], to make empirical estimates of cross sections and plasma rate coefficients directly accessible. This expansion of JAC may therefore enhance the reliability and interpretability of non-LTE plasma simulations, while keeping them practical for users.

This work is organized as follows. We first review in the next section the role of atomic data in plasma simulations and the challenges in locating and interpreting suitable datasets. We then provide a short discussion of photon and electron distributions, and how these distributions enter the definition of empirical plasma rates and rate coefficients for photon-induced processes. In Section 3, we focus on rapid access to useful empirical estimates for selected distributions and rates, illustrated by simple code examples using the JAC toolbox. Here, we explain how empirical estimates can be adapted to the context and become readily usable in non-LTE plasma simulations. Finally, a short summary and conclusions are given in Section 4.

2. Use of Atomic Data for Plasma Simulations

2.1. The Challenge of Finding the Right Data

Various advanced quantum (many-electron) techniques have been developed in the past to predict accurate atomic energies and cross sections. These methods, including the relativistic configuration-interaction and coupled-cluster approaches [14–16], have demonstrated remarkable accuracy for many-electron systems [17,18]. More often than not, however, these techniques are limited to atoms and ions with low excitation or simple shell structures near their ground state. For plasma simulations, in contrast, the practical use of atomic data is often hampered by severe difficulties. These arise from inconsistencies in how data are generated, represented, and documented across different sources [19–21]. The most relevant issues can perhaps be summarized as follows.

Inconsistent notations: Many data sources use quite different or even conflicting names and symbols to denote cross sections, plasma rates, or rate coefficients. These inconsistencies complicate the comparison of data and simulations without their careful reinterpretation.

Ambiguous or incompatible units: Many publications also use uncommon or ambiguously defined physical units. Seldom, in addition, do the units not match the quantity itself, and first require careful conversion before their use.

Lack of physical dependencies: The dependence of cross sections and plasma rates on electronic configurations, levels, temperature, or densities is often unclear or only implicitly specified, and may lead to either missing contributions or double counting in simulations.

Missing assumptions: Many empirical and semi-empirical expressions are utilized without recalling the assumptions made in their derivation. Typical assumptions concern the use of hydrogenic models, neglect of interference terms, or (very) simplified temperature

scalings. If ignored, these formulas may therefore easily be applied outside their intended parameter ranges.

Unclear data uncertainties: Uncertainty estimates are rarely provided for empirical atomic data, making it difficult to judge their reliability or to compare competing datasets. Moreover, it remains often unclear whether data are theoretical, experimental, fitted or interpolated.

Limited traceability of data: Inconsistent definitions, units, and assumptions across data sources often create a patchwork of conventions that obscure the physical origin and validity range of many datasets. Such patchworks undermine reproducibility and confidence in simulation results.

Incomplete data: Incomplete or averaged datasets can mask the role of metastable levels or specific electron configurations and may invalidate plasma simulations far from equilibrium.

All these difficulties typically reduce the accuracy and reproducibility of non-LTE plasma modeling [22–25]. They undermine confidence in computed plasma properties and make comparisons between models unreliable. These recurring difficulties have motivated us to adapt a consistent notation and to expand JAC with the aim to standardize data representations, make assumptions explicit, and to expose the essential physical dependencies as often needed for practical non-LTE plasma simulations.

2.2. Explicit Use of Photoionization and Photorecombination Plasma Rates

2.2.1. Frequently Applied Photon and Electron Distributions

The simulation of plasmas always requires knowledge of, or at least reasonable assumptions about, the underlying distribution of photons and electrons [26,27]. These distributions control the impact of individual atomic processes upon the plasma and determine its temporal evolution. In an LTE plasma, or close to such an equilibrium, the spectral energy-density of photons at temperature T follows Planck's black-body law, expressed in terms of the photon angular frequency ω as [28]

$$u^{(\text{Planck})}(\omega; T) d\omega = \frac{\hbar \omega^3}{\pi^2 c^3} \frac{d\omega}{\exp(\hbar\omega/k_B T) - 1} \quad [\text{J cm}^{-3} \text{ Hz}^{-1}], \quad (1)$$

where $\hbar \omega$ is the photon energy, c the speed of light and k_B the Boltzmann's constant. This energy density (distribution) describes the radiation that is emitted by an ideal black body in thermodynamic equilibrium. From this energy distribution, the spectral flux density $F(\omega; T) = c/(4\hbar \omega) u(\omega; T)$ [$\text{cm}^{-2} \text{ s}^{-1} \text{ Hz}^{-1}$] and the (spectral) radiance or, in short, intensity $I(\omega; T) = c/(4\pi) u(\omega; T)$ [$\text{J cm}^{-2} \text{ s}^{-1} \text{ Hz}^{-1}$] is easily obtained and is known in LTE to grow $I(\omega; T)^{(\text{Planck})} \sim \omega^2$ at low frequencies (Rayleigh–Jeans limit).

Several modified photon distributions have been applied as well in astrophysics and plasma modeling. They describe, for instance, diluted black-body fields in stellar atmospheres or the (free–free) bremsstrahlung emission from a hot, optically thin plasma featuring a rapid exponential cutoff and dominated by electron–ion collisions [29]. In non-equilibrium conditions, moreover, a power-law distribution is often adopted to approximate synchrotron or inverse-Compton emission from high-energy sources [30,31]. These alternative photon distributions enable one to account for deviations from Planckian fields and are widely applied in astrophysical and laboratory plasma models. All these photon distributions can be expressed in terms of the photon frequency ω , and they depend parametrically on the temperature T of the photon field. Table 1 lists several photon (and electron) distributions that can be utilized to compute photoexcitation and photoionization plasma rates and rate coefficients. In many cases, the spectral photon number density

$n(\omega; T) = u(\omega; T)/\hbar\omega$, rather than the spectral energy-density $u(\omega; T)$, is the physically relevant quantity, especially when stimulated processes are significant.

For photorecombination processes, in contrast, the free-electron energy (or velocity) distribution must be known at the electron temperature T_e of the plasma. The well-known Maxwell–Boltzmann distribution describes electrons with velocities near the thermal average. For fermions, this classical distribution should often be replaced by the Fermi–Dirac distribution to account for quantum statistics or, in simpler terms, Pauli’s exclusion principle. The Fermi–Dirac distribution is especially relevant in dense plasmas or degenerate matter, where available energy states are partially occupied and where classical approximations fail [32].

By providing consistent and easily accessible functions for these distributions, the JAC toolbox ensures that photon-mediated plasma rates and rate coefficients can be computed on equal terms. Apart from specifying these distributions, the user can directly set the temperatures (either T or T_e) in the plasma. Indeed, this capability is essential for reliable non-LTE plasma simulations.

Table 1. Selected photon and electron distributions implemented in the JAC toolbox for the computation of photoionization (PI), photorecombination (PR), photoexcitation (PX), and photo-de-excitation (PD) rates and rate coefficients. Apart from the function name and its (parametric) dependencies, a brief explanation is given along with just simple expressions and proportionalities, while all further details can be found in the JAC toolbox or from Julia’s help facilities (Julia comes with a full-featured interactive and command-line REPL (read-eval-print loop) that is built into the executable of the language).

Distribution, Brief Explanation and Implementation in the JAC Toolbox
PhotonPlanck(T): Planck’s black-body distribution for an equilibrium photon spectrum at (radiation) temperature T .
PhotonDilute(T; w): In stellar atmospheres, the radiation field is often approximated by a diluted black-body spectrum $u^{(Dilute)}(\omega; T, w) = w \cdot u^{(Planck)}(\omega; T)$, where $0 < w < 1$ is the geometric dilution factor. Such a diluted field preserves Planck’s spectral shape but reduces the overall photon intensity seen by the plasma.
PhotonPowerLaw(Tc, A, p, ω_{min} , ω_{max}): Photons from synchrotron or inverse Compton processes in high-energy sources exhibit a non-thermal power-law distribution $n^{(Power\ law)}(\omega; T_c, p, A, \omega_{min}, \omega_{max}) = A \omega^{-p} \exp\left(-\frac{\hbar\omega}{kT_c}\right)$ [cm ⁻³ (rad/s) ⁻¹], where p is called the spectral index, T_c a characteristic cutoff temperature (or energy-scale), and A a normalization constant. Typical additional parameters are lower/upper cutoffs ω_{min} , ω_{max} that are taken to ensure convergence and represent physical bounds.
PhotonVacuumField(T): The photon vacuum field has a zero spectral photon density $n(\omega; T) \equiv 0$, and has been found useful to evaluate spontaneous rates and rate coefficients.
ElectronMaxwell(Te): A Maxwell–Boltzmann velocity distribution of classical particles (electrons) $f_e(v; T_e) \sim v^2 \exp(-mv^2/2k_B T_e)$ that determines the probability of finding electrons with velocity v at temperature T_e .
ElectronFermiDirac(Te, μ): Electrons in degenerate or partially degenerate plasmas often follow a Fermi–Dirac distribution, $f_e(v) = [\exp[(\frac{1}{2}m_e v^2 - \mu)/k_B T_e] + 1]^{-1}$, where μ is the chemical potential.
ElectronBiMaxwellian(Te, , Te,⊥): The bi-Maxwellian distribution describes a plasma, in which the electron velocities along and perpendicular to a preferred direction (e.g., a magnetic field) have different temperatures; this is not yet well supported in JAC.

2.2.2. Photoionization Rates and Rate Coefficients

The photoionization (PI) cross section is a fundamental property that depends entirely on the electronic structure of the atom or ion, i.e., upon the energy levels, the associated wavefunctions, the polarization of the incoming photons, and on the selection rules to be considered. It is independent of plasma parameters, such as the temperature or density.

For the PI of a q -fold charged ion A^{q+} in the initial level i to the photoion $A^{(q+1)+}$ in level f , the PI cross section at the frequency ω can be expressed approximately as

$$\sigma^{(PI)}(\omega; i \rightarrow f) = 4\pi^2 \alpha \omega \sum_{\lambda} |\langle f | \mathbb{D}_{\lambda} | i \rangle|^2 \quad [\text{cm}^2]$$

in terms of the (electric-dipole) transition amplitude $\langle f | \mathbb{D}_{\lambda} | i \rangle$ and the fine-structure constant α , and by taking into account a summation over the polarization (states) of the photons. Here, the indices i and f may optionally refer to specific fine-structure levels, LS terms, or even to whole electron configurations, depending on the averaging involved into the simulations. These cross sections can readily be calculated in the JAC toolbox for most ions across the periodic table of elements [33], though often at the cost of substantial computational efforts and with limited use for plasma simulations.

A semi-empirical estimate for the PI cross section of a bound electron has been given by Bethe and Salpeter [34], based on Kramer’s formula [35]

$$\sigma^{(PI: \text{ScaledHydrogenic})}(\omega; i \rightarrow f[a]) = \frac{64\pi^2}{3\sqrt{3}} \frac{\alpha a_0^2}{n_a} \left(\frac{Z^{(\text{eff})} [\text{Hartree}]}{\hbar\omega} \right)^3 g^{(\text{bf})}(\omega),$$

where n_a refers to the principal quantum number of the photoionized shell or subshell in the final configuration f , $Z^{(\text{eff})}$ to the effective charge as seen by this electron, and $g^{(\text{bf})} \approx 1$ to the bound-free Gaunt factor, often omitted in plasma simulations. This expression was originally derived for hydrogenic ions but was adapted to other ions A^{q+} in their ground configuration. The cross section is naturally zero for photon energies below the ionization threshold, $\hbar\omega \geq E_{\text{th}} = \varepsilon_a$, e.g., the binding energy of the photoionized shell. This simple approximation captures the main scaling behavior of the PI cross section with frequency ω and the effective charge of the ion, and has often served as a first reference for many quantum mechanical calculations. In the JAC toolbox, we can readily estimate the binding energy (threshold energy) of electrons for the ionization of—valence and inner-shell—electrons. A similar form $\sigma^{(PI: \text{fitted})}(\omega, i \rightarrow f) \approx \sigma_0(i \rightarrow f) \left(\frac{E_{\text{th}}}{\hbar\omega} \right)^3$ has often been used in astrophysical modeling to express the frequency behavior or to fit the cross sections to experimental data.

The PI plasma rate coefficient $\alpha^{(PI)}(T; i \rightarrow f)$ quantifies the number of photoionization events per time unit for a single ion in level i within a (unit) volume. It provides the quantitative link between microscopic atomic processes and the macroscopic evolution of the plasma, and it describes how fast a given transition proceeds at a specified photon distribution. The PI rate coefficient is obtained from the convolution of the PI cross section with the photon number density

$$\alpha^{(PI)}(T; i \rightarrow f) = \int_0^{\infty} d\omega n(\omega, T) c \cdot \sigma^{(PI)}(\omega; i \rightarrow f) \quad [\text{cm}^3/\text{s}] \quad (2)$$

$$\alpha^{(PI)}(T; i) = \sum_f \alpha^{(PI)}(T; i \rightarrow f).$$

This rate coefficient depends directly on the spectral shape of the radiation field as characterized by the plasma temperature T and a few additional parameters [cf. Table 1], and it is closely related also to the PI plasma rate $R^{(PI)}(T; i) = n_{\text{ion}}(i) \cdot \alpha^{(PI)}(T; i) \text{ [s}^{-1}\text{]}$, if multiplied with the number density of ions being in the initial level i .

The PI plasma rate coefficient is particularly useful in non-LTE models when the radiation field is known. It allows computing the ionization rates for an ensemble of atoms or ions with different level populations [36,37]. Unlike the raw PI plasma rate,

which depends on the local intensity and ion number density, the rate coefficient cleanly separates atomic properties (via the corresponding cross section) from the explicit radiation environment by just accounting for the general photon number distribution. This separation allows its precomputation or tabulation as a function of the photon-field temperature and the ion level of interest. For a first estimate of the PI plasma rate coefficient $\alpha^{(\text{PI: ScaledHydrogenic})}(T; i \rightarrow f)$, we can use again Bethe and Salpeter’s photoionization cross section $\sigma^{(\text{PI: ScaledHydrogenic})}(T; i \rightarrow f)$ and the black-body photon distribution $n^{(\text{Planck})}(\omega, T)$ but can utilize also any other photon distributions. In these computations, it is generally enough to provide the generic photon distribution and to perform the numerical integration over ω in Equation (2) internally.

For a black-body photon field, in particular, the approximate PI plasma rate coefficient becomes [38]

$$\begin{aligned} \alpha^{(\text{PI: Planck})}(T; i \rightarrow f) &= \int_0^\infty d\omega n^{(\text{Planck})}(\omega, T) c \cdot \sigma^{(\text{PI})}(\omega; i \rightarrow f) \\ &= \int_{\omega_{\text{th}}}^\infty \frac{d\omega}{\omega} \frac{\sigma^{(\text{PI})}(\omega; i \rightarrow f)}{\exp(\hbar\omega/kT) - 1} \frac{8\pi\omega^2}{c^2}. \end{aligned}$$

This integral must be evaluated numerically for the specified plasma temperature and threshold energy ω_{th} .

2.2.3. Photorecombination Rates and Rate Coefficients

Photorecombination (PR) is the time-reversed process of PI, in which a free electron recombines with an ion under photon emission: $A^{(q+1)+} + e^- \rightarrow A^{q+} + \hbar\omega$. Since the electron can be captured into different final levels f of the recombined ion, photons with a (discrete) wide range of energies $\hbar\omega$ are typically produced.

In LTE, PI and PR cross sections are connected to each other by microscopic balance, which means that each transition from an initial bound to a free-electron state is balanced by its reverse. For the photon-mediated processes, this principle of detailed balance is formally described by the Einstein–Milne relation [39,40] and based on the three well-known (classical) LTE distributions: (i) an ambient black-body radiation field, (ii) a Maxwellian electron distribution, and (iii) a Boltzmann distributed level population. Following the Einstein–Milne relation, the PR and PI cross sections are linked by

$$\sigma^{(\text{PR: spontaneous})}(\varepsilon; i \rightarrow f) = \frac{g_f}{g_i} \frac{2\pi^2 c^2}{2\hbar\omega^2} \sigma^{(\text{PI})}(\omega; f \rightarrow i), \tag{3}$$

where the kinetic energy of the free electron ε and the photon energy $\hbar\omega$ are fixed to each other by $\varepsilon = \hbar\omega - (E_f - E_i)$. Obviously, the PI cross sections $\sigma^{(\text{PI})} \equiv \sigma^{(\text{PI: stimulated})}$ always refer to a stimulated process. For the PR, however, we need to distinguish between the spontaneous and stimulated recombination due to the ambient radiation field. Apart from the cross sections, of course, the same distinction needs to be made also for the associated plasma rates and rate coefficients $\alpha^{(\text{PR})}(T; i \rightarrow f)$ [41].

In expression (3) for the PR cross sections above, we can readily sum again over the final states f , although this should include only the recombination into valence-shell excitations since the inner shells are already occupied. This difference in the admissible initial and final levels causes a subtle yet important distinction to connect PI and PR cross sections. In PI, the initial state is typically a ground or low-lying metastable level, and the ionization may involve also inner-shell electrons. In contrast, PR involves the capture of a free electron into an available bound state, in which all inner shells are already occupied. When using the Einstein–Milne relation to derive PR cross sections from PI data, one must

carefully restrict the summation to physically allowed recombination channels. Failing to account for this subtlety can lead to the overestimation of PR rates, especially in multi-electron ions with a complex inner-shell structure, a concern that has hardly been discussed in the literature.

In fact, the PR process usually requires further care, as the recombination can occur not only as spontaneous or stimulated but may proceed also either directly (via radiative recombination: RR) or dielectronic recombination (DR). All these four combinations (direct-spontaneous, direct-stimulated, ...) above will generally occur in a plasma. In RR, a free electron is captured directly into a bound state of the ion under the emission of a photon. In DR, on the other hand, the electron is first captured into an intermediate (Rydberg) state, while a bound electron is simultaneously excited; the system then stabilizes through radiative decay. In practice, these two processes can usually be treated as additive: RR dominates at low electron temperatures and for light elements, whereas DR becomes important at higher temperatures or for ions with closely spaced excited states.

To briefly recall, spontaneous PR occurs when a free electron is captured by an ion and directly emits a photon without an external radiation field. This emission is an intrinsic radiative process that arises from the interaction of the free electron with the ion and the quantized electromagnetic field. In contrast, the stimulated PR occurs in the presence of a photon field, which increases the emission probability and produces photons that are coherent with the ambient field. For low photon densities $n(\omega; T) \ll 1$, the spontaneous PR dominates, while stimulated PR may increase significantly the total rates at high photon densities.

From the spontaneous PR cross sections (3), the associated plasma rate coefficient is obtained by averaging over the electron energy distribution $f_e(\varepsilon; T)$ at the given (electron) temperature of the plasma:

$$\alpha^{(\text{PR: spontaneous})}(T_e; i \rightarrow f) = \int_0^\infty d\varepsilon f_e(\varepsilon; T) v(\varepsilon) \sigma^{(\text{PR: spontaneous})}(\varepsilon; i \rightarrow f) \text{ [cm}^3/\text{s]},$$

where $v(\varepsilon)$ is the electron velocity. These coefficients can be comprised into rate coefficients $\alpha^{(\text{PR: spontaneous})}(T_e; i)$ by a summation over the final levels f but by including the arguments from above. From these spontaneous PR rate coefficients, the total coefficient can be obtained by

$$\alpha^{(\text{PR: total})}(T_e; n(\omega; T); i \rightarrow f) = \alpha^{(\text{PR: spontaneous})}(T_e; i \rightarrow f) [1 + n(\omega; T)] \text{ [cm}^3/\text{s]}, \tag{4}$$

with analogue constraints with regard to the desired summation over final levels f .

To finally derive the PR rates [1/s], either spontaneous, stimulated, or total rates, a free electron and an ion must meet and, hence, the rate will depend on both densities. In practice, the physically meaningful quantity is then the (so-called) event rate per unit volume: $R^{(\text{PR})}(T_e; n(\omega; T); i \rightarrow f) / V = n_e \cdot n_{\text{ion}}(i) \cdot \alpha^{(\text{PR})}(T_e; n(\omega; T); i \rightarrow f)$. Together with Equation (4), the spontaneous PR cross sections and rate coefficients are therefore central, and must be combined consistently with the local electron density and photon flux to yield physically meaningful total rates in the associated rate equations. The total PR rate therefore depends on (i) the electron density and temperature, (ii) the photon radiation temperature, and (iii) the detailed atomic level structure of the recombining ion through the energy-dependent cross sections. They are all usually computed ad hoc in plasma codes. For isotropic black-body radiation, the stimulated contribution scales approximately with $n^{(\text{Planck})}(\omega; T)$ and becomes significant at infrared and microwave frequencies.

Explicit (expressions and) numerical routines are provided in the JAC toolbox for $\sigma^{(\text{PR: spontaneous})}(\varepsilon; i \rightarrow f)$ and $\alpha^{(\text{PR: spontaneous})}(T_e; i \rightarrow f)$ for any of the supported

electron distributions but, to date, based on *scaled-hydrogenic* PI cross sections as well as the Einstein–Milne relation (3), special care has to be taken if any of these assumptions are not appropriate for the considered non-LTE conditions. In general non-LTE plasmas, the underlying distributions are no longer valid.

2.2.4. Photoexcitation and Photo-de-Excitation Rates

Photoexcitation (PX) and photo-de-excitation (PD) are radiative bound–bound processes that strongly affect the population balance among atomic or ionic levels, especially under non-LTE conditions. In (stimulated) PD, an external photon induces the transition back from—a previously excited—level $f \rightarrow i$ under the coherent emission of a photon with the ambient field. In a plasma, of course, we need to distinguish again between the spontaneous and stimulated PD in order to account for the intrinsic coupling of the atom to the vacuum field. In thermal equilibrium, as before, the rates of these—spontaneous and stimulated—processes must balance in such a way that Planck’s black body distribution is obtained. This requirement has led to the well-known Einstein coefficients for (stimulated) absorption, stimulated emission, and spontaneous emission, which form a cornerstone of modern radiation–matter interaction theory.

Similar to those in PR, the (spontaneous) PD and PX cross sections and rates are related through the Einstein–Milne relation or, more explicitly, the ratio of the corresponding Einstein A and B coefficients. These coefficients satisfy the detailed-balance relations

$$A(i \rightarrow f) = \frac{2 \hbar \omega^3}{\pi c^3} B(i \rightarrow f), \quad g_i B(i \rightarrow f) = g_f B(f \rightarrow i),$$

if g_i and g_f denote the degeneracies of the associated levels (configurations). Again, these Einstein coefficients depend entirely on the electronic structure of the atoms and ions, especially the transition dipole moments and selection rules, but are independent of the surrounding plasma.

In a plasma, the rate per atom or ion provides again the link between elementary processes and the (macroscopic) evolution of the plasma; it describes how fast a given transition proceeds for a single ion and a specified photon distribution. These rates are

$$\begin{aligned} R^{(\text{PD: spontaneous, per ion})}(T; i \rightarrow f) &\equiv A(i \rightarrow f) && [\text{cm}^{-3}] \\ R^{(\text{PD: total, per ion})}(T; i \rightarrow f) &= A(i \rightarrow f) [1 + n(\omega_0; T)] \\ R^{(\text{PX, per ion})}(T; i \rightarrow f) &= \frac{g_f}{g_i} A(f \rightarrow i) n(\omega_0; T), && \omega_0 = E_f - E_i \\ R^{(\text{PX})}(T; i \rightarrow f) &= n_\gamma R^{(\text{PX, per ion})}(T; i \rightarrow f), && n_\gamma = \int d\omega n(\omega; T). \end{aligned}$$

The factor $n(\omega_0; T)$ appears because the probability for induced emission is proportional to the number of photons in the corresponding radiation mode. The relations above assume isotropic radiation as well as a constant photon field over the line profile $L(\omega)$ of the given transition. All these relations are analogue to the bound-free (PI) transitions but with the appropriate density of bound states and slightly different pre-factors. In non-LTE plasmas, as before, their relative rates depend on the actual photon distribution and level populations.

The discrete level structure of atoms complicates (and makes it less relevant) to formulate PX cross sections and plasma rate coefficients as the cross sections typically appears in convolution with the photon number density $n(\omega; T)$. This convolution simplifies for a monochromatic photon field at $\omega = \omega_0$ to $\alpha^{(\text{PX})}(T; i \rightarrow f) = c \cdot \alpha^{(\text{PX})}(\omega_0; i \rightarrow f) [\text{cm}^3 \text{s}^{-1}]$ and $R^{(\text{PX})}(T; i \rightarrow f) = n_\gamma \cdot \alpha^{(\text{PX})}(T; i \rightarrow f)$ if $n_\gamma [\text{cm}^{-3}]$ the total photon number density.

The PX cross-section and rate coefficients can be related also to the Einstein $A(f \rightarrow i)$ coefficient for bound-bound transitions with a Lorentzian profile and the widths Γ [eV]

$$\alpha^{(\text{PX: Lorentzian})}(T; i \rightarrow f) = c \cdot \sigma^{(\text{PX})}(\omega_0; i \rightarrow f) = \frac{2c^3}{\omega^2} \frac{g_f}{g_i} \frac{A(f \rightarrow i)}{\Gamma} \quad [\text{cm}^3 \text{s}^{-1}].$$

For a broad-band field, the convolution $\alpha^{(\text{PX})}(T; i \rightarrow f) \propto \int d\omega n(\omega; T) \sigma^{(\text{PX})}(\omega; i \rightarrow f)$ must be evaluated again numerically.

Empirical Einstein $A(i \rightarrow f) \equiv A_{if}$ coefficients provide a practical way to estimate radiative rates when full quantum calculations are unavailable. Scaling relations along isoelectronic sequences have been widely used for rapid estimates of Einstein A coefficients along isoelectronic sequences [42,43], although these expressions become usually inaccurate in dense or strongly radiating environments, under extreme temperatures, or when many-body contributions modify the level populations. We can apply again scaled-hydrogenic dipole expressions or fast estimations from the JAC code, in which the initial and final level indices $i \rightarrow f$ capture the main dependence on the energy and effective charge of these A coefficients. They are valid for single-electron or weakly perturbed systems but often lose relevance for ions with open shells or strong configuration mixing, i.e., when strong electron correlations, relativistic effects, or highly excited levels dominate. In these cases, detailed quantum calculations or tabulated data are required. Explicit dependencies of the plasma rates and rate coefficients on initial and final levels, transition energy, and the photon distribution must always be specified in order to avoid misapplication in non-LTE simulations.

2.2.5. Other Photo-Induced Ionization and Recombination Processes in a Plasma

In addition to the standard PX and PI processes, and their time-reversed PD as well as PR mechanisms from above, a variety of more complex photon-induced processes can occur in plasma owing to the coupling with intense electron beams or specifically structured radiation fields [44]. Among these is the photo-double ionization, where a single photon simultaneously ejects two electrons, a process that depends on sufficiently high photon energies and electron correlations. Another important but often omitted channel is photoexcitation with subsequent autoionization, also called resonant photoionization [45,46], which proceeds through intermediate resonant states and contributes significantly to the ionization balance in highly excited ions [47]; it is the time-reversed process to the DR mentioned above. Moreover, various shake-up and shake-off processes can occur in a plasma, if the atomic potentials change rapidly so that other electrons are excited or ejected. Such many-body contributions to the plasma rates become relevant in high-energy-density or highly ionized plasmas, where correlation and relaxation phenomena can no longer be neglected. Although these mechanisms are usually (much) weaker than standard PI under moderate conditions, they can become dominant in strongly irradiated plasmas, such as those exposed to short-wavelength, high-intensity radiation. In addition, these higher-order processes influence not only the charge state of ions but also the re-emitted photon distribution in a plasma.

Finally, various collisional processes provide further competition to photon-driven mechanisms. Electron-impact excitation and ionization occur when energetic free electrons transfer kinetic energy to bound electrons, inducing level excitation or ejection. At high electron densities and temperatures, these collisional processes often dominate, whereas photoexcitation and photoionization prevail in low-density, radiation-rich environments. Three-body recombination becomes important when two electrons interact with an ion in such a way that one of them is captured, while the other carries away the excess energy. A good understanding of the balance between radiative and collisional mechanisms

is essential for the realistic modeling of non-LTE plasmas and for interpreting spectral diagnostics that depend sensitively on the dominant excitation and ionization channels.

2.3. Implementation and Use of Empirical Expressions and Estimates

Detailed quantum mechanical data for cross sections, plasma rates and rate coefficients are unavailable for most ions or specific transitions $i \rightarrow f$ of interest. In such cases, (semi-) empirical expressions and estimates provide a rapid and practical access to approximate atomic data, often sufficient for exploratory or basic plasma simulations. In practice, however, the use of these estimates still depends critically on the underlying assumptions, their range of validity, and the consistent treatment of physical units [48]. Because most empirical formulas were derived for simplified shell structures and/or idealized plasma conditions, they should be applied with reasonable precautions and verified against available benchmark data, whenever feasible. Here, the consistent notation and explicit definition of all quantities within the JAC toolbox help to overcome these difficulties and to ensure a transparent, reproducible use of empirical data. With the present expansion, therefore, JAC aims for fast and physically meaningful access to approximate atomic data for non-LTE and radiation-driven plasma simulations.

This goal can be illustrated, for instance, by estimating the PI or PR plasma rate coefficient for an ion that is exposed to a photon field with spectral number density $n(\omega; T)$, cf. Equation (2). In JAC, the rate coefficient $\alpha^{(\text{PI})}(T; i \rightarrow f)$ can be obtained interactively by just providing the photon distribution at some given temperature as well as the configurations of the initial and final states:

```
T_au = 1.0 # photon-field temperature in [a.u.]; 1 a.u. = 3.157 * 10-5 K
photonDist = Distribution.PhotonPlanck(T_au)
piRate = Empirical.photoionizationPlasmaAlpha(photonDist, iConf, fConf, ...)
```

for any supported photon distribution `photonDist`. Similarly, a PR rate coefficient $\alpha^{(\text{PR:spontaneous})}(T; i \rightarrow f)$ is obtained by selecting a proper electron distribution

```
Te_au = 1.0 # electron temperature in [a.u.]
electronDist = Distribution.ElectronMaxwell(Te_au)
pxRate = Empirical.photorecombinationPlasmaAlpha(electronDist, iConf, fConf, ...)
```

The clear separation between the cross section and the radiation or electron field, internally described by the photon number density $n(\omega; T, \dots)$ or electron distribution $f_e(v; T, \dots)$ enables one to flexibly integrate these rate coefficients into plasma-simulation workflows.

Let us conclude this section with an important caveat. We do not attempt to derive or rigorously justify the empirical expressions behind the implemented cross sections, nor to provide a complete set of (Julia) functions for all possible photo-induced processes. Instead, our focus is on their systematic and transparent implementation within the JAC toolbox. Section 3 presents selected examples which illustrate both the required input and parts of the resulting output from this toolbox. By incorporating the toolbox and these empirical cross sections and rates into JAC, users can compare different models, assess underlying assumptions, and more easily identify potential limitations. This approach is particularly valuable in cases where detailed atomic data are unavailable or when their computation (or extraction from existing databases) would be prohibitively expensive.

3. Rapid Access to Useful Empirical Estimates

Accurate atomic (structure) calculations usually provide data for only a limited set of ions, transitions, or plasma conditions at any given time. They are often stored in specialized

databases that may be fragmented or inconsistently formatted, making them difficult to access efficiently during plasma simulations [4,49]. Moreover, these detailed results often obscure explicit dependencies on physical quantities, such as the level structure, temperature, or radiation intensity, but which are crucial for transparent interpretation and reproducible modeling.

For practical plasma modeling, especially in non-LTE environments, rapid and transparent access to key quantities, such as cross sections and rate coefficients, appears mandatory. The JAC toolbox therefore offers both a consistent notation and a modular structure to support this request. Below, we first outline the concept of this toolbox and then illustrate how it enables quick admittance to relevant plasma quantities.

3.1. Brief Overview to the JAC Toolbox—Towards the Use of Empirical Expressions

JAC, the Jena Atomic Calculator, is a computational toolbox that supports the atomic structure, process, and cascade calculations of different complexities [12,13,50]. These tools apply configuration-interaction and multi-configuration Dirac–Fock–Slater wavefunctions to approximate bound states and transition amplitudes, suitable especially for medium to heavy elements [51]. JAC’s modular design and easy control facilitates computing level energies, cross sections and various decay rates, both radiative and non-radiative. The JAC toolbox has been documented in previous works and is available for download [52], including the present extension.

JAC now supports also a simple and rapid access to (semi-) empirical estimates. However, these estimates can differ significantly from accurate electronic-structure calculations and, hence, were not in the focus of JAC’s original design. Nonetheless, they (may) become valuable when modeling atomic behavior in complex plasmas with multiple processes, charge states, or ion types. These estimates are usually based on parametrized formulas for approximate cross sections, plasma rates, and rate coefficients under certain assumptions. Emphasis is placed on providing consistent and explicit notations that allow comparison of models, tracking of assumptions, and direct use in non-LTE plasma simulations. Apart from a few abstract and concrete data types [cf. Figure 1], distinguishing commonly used empirical distributions and approximations, no additional data structures were added, keeping these tools straightforward and easy to use.

Most empirical expressions implemented in this extension have been taken from the literature, sometimes with limited information about their physical assumptions, derivations, or validity ranges. These limitations make it hard to determine the justification and applicability of individual approximations for specific plasma conditions. The transparent and unified notations in this work, however, help users to utilize and compare different estimates, and to apply them critically and more consistently. In the following, we shall mainly illustrate how readily selected plasma rates and rate coefficients can be generated and explored interactively within JAC.

3.2. Selecting Useful Photon and Electron Distributions

To account for the plasma environment, one usually needs to select and specify the distribution function of the surrounding photons and electrons. These distributions enter directly into the convolution of the cross sections in order to compute the plasma rates and rate coefficients. Often, however, users may wish to apply these distributions without computing the convolution explicitly, i.e., without tracking the full distribution functions. In the JAC toolbox, we support this approach by providing generic data types for selected photon and electron distributions, a feature that keeps the input readily controllable. It also allows the easy addition of further distributions to the code, if the need arises.

```

abstract type Distribution.AbstractPhotonDistribution
... defines an abstract and a number of singleton types to deal with different electron and
photon number distributions in a plasma [cf. Table 1].

+ PhotonDilute          ... to apply a dilute photon distribution.
+ PhotonPlanck          ... to apply Planck's black-body photon distribution.
+ PhotonPowerLaw        ... to apply a power-law photon distribution.
+ PhotonVacuumField     ... to apply a vacuum (zero-intensity) photon distribution.

struct PhotonPlanck <: Distribution.AbstractPhotonDistribution
... to apply Planck's black-body photon spectrum to photoexcitation, photonionization, and
recombination processes.

+ T                    ::Float64 ... temperature

abstract type Empirical.AbstractEmpiricalApproximation
... defines an abstract as well as a number of singleton types to deal with different empirical
approximation for deriving the cross section and rates of photon-mediated processes.

+ ScaledHydrogenic     ... if hydrogenic expressions are scaled to compute cross sections.
+ UsingJAC              ... if simple mean-field computations are used to generate energies and
single-electron wave functions to estimate cross sections.

```

Figure 1. Definition of the data structures `Distribution.AbstractPhotonDistribution` (upper panel), `Distribution.PhotonPlanck` (middle panel) and `Empirical.AbstractEmpiricalApproximation` (lower panel) that all facilitate the computation of empirical plasma rates and rate coefficients. The distributions are specified by generic functions that can be passed to different (compute) functions, which then evaluate the convolution with these distributions numerically. Moreover, the empirical cross sections or rates are determined by an explicitly selected or default approximation `<: Empirical.AbstractEmpiricalApproximation`, which enables one to readily add further approximations to the code. See text for further explanations.

To deal with different photon and electron distributions in a plasma, the abstract (data) type `Distribution.AbstractPlasmaDistribution` has been defined, along with several concrete types, such as `PhotonPlanck`, `PhotonDilute`, or `ElectronMaxwell`. Table 1 shows several of these distributions, along with a brief explanation of their physical background and the name (convention) used within the JAC toolbox. These distributions cover a good range of plasma environments, from thermal black-body radiation to degenerate electron (energy) distributions. They typically request to provide the plasma temperature, and perhaps further parameters that make the distribution unique, but not the photon frequency or electron velocity, over which one needs to integrate in the plasma rates. These data types can therefore be passed directly to functions that compute PI, PR, or PX rates and rate coefficients, and they ensure that the distribution is used consistently. They also enable one to readily “switch” between different distributions, for instance in order to compare Maxwellian and Fermi–Dirac electron velocities. This modular approach simplifies the evaluation of plasma rates and rate coefficients in non-LTE simulations, while keeping the interface clear and flexible.

3.3. Photoionization Cross Sections and Plasma Rate Coefficients

Let us start with the concept of PI rates and rate coefficients for carbon-like neon in their ground configuration. Representative values of photoionization plasma rates have been reported in the literature for a few simple atomic systems, most notably for hydrogen and hydrogen-like ions. Early examples include prior calculations of photoionization rates from the $1s$ ground level of H I and He II in black-body radiation fields at various temperatures [30,40]. In these studies, Kramers’ cross sections were combined with Planck’s photon distribution to obtain temperature-dependent rates, often presented or illustrated for radiation temperatures between 10^4 and 10^6 K. The tables in Ref. [40,53,54] provide reference

data for the direct comparison and benchmarking of approximate rate coefficients, serving as a selected example for hydrogenic photoionization under astrophysical conditions.

In the JAC toolbox, “hydrogenic” cross section, but scaled for atoms and ions in some general configurations $i \rightarrow f$, can be accessed by calling

```

setDefault("unit: cross section", "barn")
setDefault("unit: energy", "eV")
setDefault("nuclear: charge", 10.0)
iConf = Configuration("[He] 2s^2 2p^2")
fConf = Configuration("[He] 2s^2 2p")
omega = 7.0          # omega = 190.48 eV
Empirical.photoionizationCrossSection(omega, iConf, fConf, printout=true)

* Estimate empirically the photoionization cross section for a given transition i -> f with the
following assumptions/simplifications:
+ Use a simple hydrogenic scaling of the PI cross section following Bethe-Salpeter (1957).
+ Hydrogenic estimate of the binding energy (photoionization threshold) with Z^(eff) = 5.0
+ iConf = Configuration: 1s^2 2s^2 2p^2 --> fConf = Configuration: 1s^2 2s^2 2p^1
+ Binding energy of 2p = 170.071162625 eV
+ Omegas [eV] = [190.47970214]
+ Cross sections [barn] = [8.840592417940214e6]

0.3157032865333315

```

where we first define the units for the printout of final results as well as the charge of the ion ($Z = 10.0$). We here also set the configuration and the photon energy to be used in this empirical estimate. The PI cross section is computed by a call of `Empirical.photoionizationCrossSection()` in which the `approx = Empirical.ScaledHydrogenic()` is used as a default approximation. The PI cross sections are then considered for an ion with nuclear charge Z and an electron, whose initial shell is derived from the difference of occupation numbers in the initial- and final-state configurations, `iConf` and `fConf`, respectively. The parameter `printout=true` ensures that the underlying assumptions and input data are printed in the desired format. This printout can be suppressed and other approximations applied or even added to the code, if this appears useful.

This example just returns a single PI cross section in atomic units [a_0^2], independent of what is displayed otherwise on screen. We can combine such cross sections with a given photon distribution, for instance Planck’s black-body field $n^{(\text{Planck})}(\omega; T)$ to compute the associated plasma rate coefficient $\alpha^{(\text{PI:Planck})}(T; i \rightarrow f)$ at temperature $T \approx 3.16 \times 10^5$ K. This is obtained by following the short script

```

photonDist = Distribution.PhotonPlanck(1.0)
Empirical.photoionizationPlasmaAlpha(photonDist, iConf, fConf, printout=true)

* Estimate empirically the photoionization plasma rate coefficient alpha for a given transition
i -> f with the following assumptions/simplifications:
+ Photon field follows a Distribution.PhotonPlanck(1.0) at temperature T [K] = 315774.64.
+ PI cross sections are generated in the Empirical.ScaledHydrogenic() approximation.
+ iConf = Configuration: 1s^2 2s^2 2p^2 --> fConf = Configuration: 1s^2 2s^2 2p^1
+ Plasma rate coefficient alpha^(PI) [cm^3/s] = 1.333627734870559e-18

2.1769392407550897e-10

```

if we still use the default settings from above. Since the plasma rate coefficient $\alpha^{(\text{PI})}(T; i \rightarrow f)$ refers in Equation (2) to a convolution over the photon number density $n(\omega; T)$, a convenient short-cut to the computation of a whole list of cross sections is provided internally by multiple dispatch, i.e., by a method with different number or sequence of parameters. Of course, very analogue calls can be made for other photon-mediated cross sections and rate coefficients as well as photon and electron distributions. Several of these functions, currently implemented in JAC, are summarized in Table 2, along with a brief

explanation and a short description of the required parameters. The table also indicates how further functions and properties could be extended within JAC, if appropriate. All functions follow a largely consistent naming scheme, use Julia’s multiple-dispatch mechanism, and document internally the underlying approximations and limitations.

Table 2. Selected functions from the JAC toolbox for computing empirical cross sections, plasma rates, and rate coefficients. Each function can be invoked interactively or within a script to provide quick access to approximate atomic data, based on simple empirical expressions, or by performing fast mean-field computations with JAC, cf. the approximation `UsingJAC`. The (physical meaning and sequence of) parameters and their data type determine together which method of the given function is applied eventually, following Julia’s multiple-dispatch mechanism. All quantities are internally always treated in atomic units but can be readily re-expressed (and are printed) in user-defined units.

Function and Brief Explanation
<code>Empirical.photoemissionEinsteinA(iConf, fConf, approx, ...)</code> : to estimate the photonemission Einstein coefficient $A(i \rightarrow f)$ for the transition $i \rightarrow f$. Different approximations <code>approx</code> can be used for this estimation.
<code>Empirical.photoexcitationPlasmaRatePerIon(dist, iConf, fConf, ...)</code> : to estimate the PX plasma rate per ion $R^{(PX:perion)}(T; i \rightarrow f)$ for the transition $i \rightarrow f$ and for a given photon-field distribution $n(\omega; T)$ at temperature T as specified by the given distribution <code>dist</code> .
<code>Empirical.photodeexcitationPlasmaRatePerIon(dist, iConf, fConf, ...)</code> : to estimate the PD plasma rate per ion $R^{(PD:spontaneous,perion)}(T; i \rightarrow f)$ for the transition $i \rightarrow f$ and for a given photon-field distribution $n(\omega; T)$ at temperature T as specified by the given distribution <code>dist</code> .
<code>Empirical.photoionizationCrossSection(omega, iConf, fConf, ...)</code> : to estimate the PI cross section $\sigma^{(PI)}(\omega; i \rightarrow f)$ for the transition $i \rightarrow f$ at frequency $\omega \geq \omega_{th}$. A zero cross section is returned for $\omega < \omega_{th}$.
<code>Empirical.photoionizationPlasmaAlpha(dist, iConf, fConf, ...)</code> : to estimate PI plasma rate coefficients $\alpha^{(PI)}(T; i \rightarrow f)$ for the transition $i \rightarrow f$ and the given photon-field as specified by <code>dist</code> .
<code>Empirical.photorecombinationCrossSection(epsilon, iConf, fConf, ...)</code> : to estimate the (spontaneous) PR cross section $\sigma^{(PR:spontaneous)}(\epsilon; i \rightarrow f)$ for the transition $i \rightarrow f$ at the free-electron energy ϵ , based on the Einstein–Milne relation.
<code>Empirical.photorecombinationPlasmaAlpha(dist, iConf, fConf, ...)</code> : to estimate the (spontaneous) PR plasma rate coefficient $\alpha^{(PR:spontaneous)}(T; i \rightarrow f)$ for the transition $i \rightarrow f$ and for a given electron distribution $f_e(v; T)$ as specified by <code>dist</code> .

3.4. Photorecombination Plasma Rates and Rate Coefficients

Analogous to PR as the time-reversed PI process, we can deal with the photon-mediated transition $i \leftarrow f$ and compute the spontaneous PR plasma rate $\alpha^{(PR:spontaneous)}(T_e; f \rightarrow i)$. These computations follow a very similar script as before

```
electronDist = Distribution.ElectronMaxwell(1.0)
Empirical.photorecombinationPlasmaAlpha(electronDist, fConf, iConf, printout=true)

* Estimate empirically the (spontaneous) photorecombination plasma rate coefficient alpha for
a given transition i -> f with the following assumptions/simplifications:
+ Electron field follows a Distribution.ElectronMaxwell(1.0) at temperature T [K] = 315,774.64.
+ Spontaneous PR cross sections are generated in the Empirical.ScaledHydrogenic() approximation.
+ iConf = Configuration: 1s^2 2s^2 2p^1 --> fConf = Configuration: 1s^2 2s^2 2p^2
+ Plasma rate coefficient alpha^(PR: spontaneous) [cm^3/s] = 1.0983778064578154e-5

1792.930429933355
```

where the settings of the nuclear charge Z and the configurations $f \rightarrow i$ are taken (over) from above. The computations of these plasma rate coefficients are internally traced back by the Einstein–Milne relation to the computation of PI cross sections (as above)

but now convoluted over a Maxwell distribution of electrons. At present, the scaled-hydrogenic approximation adopts binding and threshold energies, useful for many-electron configurations, but does not include the DR contributions as well as the capture into excited levels of the ions. Since the low-lying DR resonances can significantly enhance the recombination rate near threshold, empirical PR rate coefficients may be inaccurate at low electron energies. At higher electron energies, the total PR rate coefficients are more reliable, as high-lying resonances contribute less significantly.

3.5. Plasma Parameters for Collisional Processes

In addition to all the photo-induced processes from above, plasmas also feature collisional processes that compete directly with radiative mechanisms. These collisional processes include electron-impact excitation and ionization, three-body recombination, and several others. Each of these processes depends explicitly on the electron distribution within the plasma and can be characterized by plasma rate coefficients in close analogy to those introduced for photon-driven reactions. Understanding the balance between radiative and collisional channels is crucial for non-LTE plasma modeling since the time evolution depends on electron and ion densities, temperatures, and the ambient radiation field.

Although the current implementation in JAC primarily focuses on photon-induced processes, a few empirical approximations for collisional rates are already available. These functions provide users with preliminary tools to explore collisional effects without requiring detailed quantum calculations. This collection is currently rather incomplete but will be enlarged so that users can perform more complete plasma simulations combining radiative and collisional processes.

4. Summary and Conclusions

We have expanded the JAC toolbox to provide rapid access to empirical cross sections, plasma rates, and rate coefficients, with particular emphasis on photoionization and photorecombination processes. Specifically, we have compiled and implemented a selection of empirical approximations and expressions known from the literature and have combined them with typical photon or electron distributions. To make the underlying assumptions and dependencies transparent, special attention has been paid to a clear and consistent notation that links atomic structure with the properties of the plasma. While our coverage is necessarily incomplete, this work provides a practical toolset for diverse plasma simulations, allowing users to handle processes for atoms and ions with complex shell structures.

Many issues from the above, including the dependence of plasma rates and rate coefficients, units or the use of different distributions, have been discussed previously. However, much of this information is often scattered throughout the literature, making it difficult to access consistent and detailed values in a unified manner. Furthermore, communication between the producers of atomic data and astrophysical modelers has remained limited, as the two communities often rely on different assumptions and implicit background knowledge, which is not immediately available to the other side. Therefore, a consistent notation can be seen as a *key* to better link the ionic level structure to plasma simulations. The present framework also facilitates the reliable addition of new processes into existing simulation codes.

Author Contributions: Conceptualization, S.F.; software, S.F. and A.K.S.; validation, S.F. and H.H.; writing—original draft preparation, S.F.; writing—review and editing, S.F., H.H. and A.K.S. All authors have read and agreed to the published version of the manuscript.

Funding: This research has been funded in part by the German Federal Ministry for Research, Technology and Space (BMFTR) within the ErUM-Pro funding scheme under contracts 05P24RG2 and 05P24SJA.

Data Availability Statement: The original contributions presented in this study are included in the article. Further inquiries can be directed to the corresponding author.

Acknowledgments: During the preparation of this manuscript, the authors used GPT-5 for the purposes of English improvement and consistency checks. The authors have reviewed and edited the output and take full responsibility for the content of this publication.

Conflicts of Interest: The author declares no conflicts of interest.

References

1. Rodríguez, R.; Espinosa, G.; Gil, J.M. Radiative properties for astrophysical plasma mixtures in nonlocal thermodynamic equilibrium. *Phys. Rev. E* **2018**, *98*, 033213. [CrossRef]
2. Holladay, D.A. An accelerated approach to inline non-LTE modeling. *J. Quant. Spectrosc. Radiat. Transf.* **2020**, *240*, 106642. [CrossRef]
3. Paletou, F.; Peymirat, C. Full non-LTE spectral line formation—I. Setting the stage. *Astron. Astrophys.* **2021**, *649*, A165. [CrossRef]
4. Summers, H.P. The ADAS User Manual, Version 2.6. 1996. Available online: <http://www.adas.ac.uk> (accessed on 10 December 2025).
5. Orban, C.; Fatenejad, M.; Lamb, D.Q. Code-to-code comparison and validation of the radiation-hydrodynamics capabilities of the FLASH code using a laboratory astrophysical jet. *Phys. Plasmas* **2022**, *29*, 053901. [CrossRef]
6. Morris, S.; Gericke, D.O.; Fritzsche, S.; Machado, J.; Santos, J.P.; Afshari, M. Recombination effects in laser-driven acceleration of heavy ions. *Phys. Rev. E* **2025**, *111*, 065209. [CrossRef]
7. Hauschildt, P.H.; Baron, E. Non-LTE treatment of Fe II in astrophysical plasmas. *J. Quant. Spectrosc. Radiat. Transf.* **1995**, *54*, 987. [CrossRef]
8. Scott, H.A. Non-LTE radiation transport in high radiation plasmas. *High Energy Density Phys.* **2005**, *1*, 31. [CrossRef]
9. Ferland, G.J. The ionization balance of a non-equilibrium plasma. *Astron. Astrophys.* **2009**, *500*, 299. [CrossRef]
10. Barfield, W.D. Partial photoionization cross sections and radiative recombination rate coefficients for lithium-like ions. *Astrophys. J.* **1979**, *29*, 856. [CrossRef]
11. Badnell, N.R. Radiative recombination data for modeling dynamic finite-density plasmas. *Astr. Astrophys. Suppl. Ser.* **2006**, *167*, 334. [CrossRef]
12. Fritzsche, S. A fresh computational approach to atomic structures, processes and cascades. *Comput. Phys. Commun.* **2019**, *240*, 1. [CrossRef]
13. Fritzsche, S.; Sahoo, A.K.; Sharma, L.; Wu, Z.W.; Schippers, S. Merits of atomic cascade computations. *Eur. Phys. J. D* **2024**, *78*, 75. [CrossRef]
14. Johnson, W.R. *Atomic Structure Theory: Lectures on Atomic Physics*; Springer: Berlin/Heidelberg, Germany, 2007.
15. Grant, I.P. *Relativistic Quantum Theory of Atoms and Molecules: Theory and Computation*; Springer: Berlin/Heidelberg, Germany, 2007.
16. Eliav, E.; Fritzsche, S.; Kaldor, U. Electronic structure theory of the superheavy elements. *Nucl. Phys. A* **2015**, *944*, 518. [CrossRef]
17. Froese Fischer, C. Multiconfiguration Hartree-Fock Breit-Pauli results for $^2P_{1/2} - ^2P_{3/2}$ transitions in the boron sequence. *J. Phys. B At. Mol. Phys.* **1983**, *16*, 157. [CrossRef]
18. Fritzsche, S. Large-scale accurate structure calculations for open-shell atoms and ions. *Phys. Scr.* **2002**, *T100*, 37. [CrossRef]
19. Grant, C.S.; Accomazzi, A.; Eichhorn, G.; Kurtz, M.J.; Murray, S.S. The NASA astrophysics data system: Data holdings. *Astron. Astrophys. Suppl. Ser.* **2000**, *143*, 111–135. [CrossRef]
20. Pepe, A.; Goodman, A.; Muench, A.; Crosas, M.; Erdmann, C. How do astronomers share data? Reliability and persistence of datasets linked in AAS publications and a qualitative study of data practices among US astronomers. *PLoS ONE* **2014**, *9*, e104798. [CrossRef] [PubMed]
21. Rosmej, F.B.; Vainshtein, L.A.; Astapenko, V.A.; Lisitsa, V.S. Statistical and quantum photoionization cross sections in plasmas: Analytical approaches for any configurations including inner shells. *Matter Radiat. Extrem.* **2020**, *5*, 064202. [CrossRef]
22. Hansen, S.; Armstrong, G.S.J.; Bastiani-Ceccotti, S.; Bowen, C.; Chung, H.-K.; Colgan, J.P.; de Dortan, F.; Fontes, C.J.; Gilleron, F.; Marquès, J.-R.; et al. Testing the reliability of non-LTE spectroscopic models for complex ions. *High Energy Density Physics* **2013**, *3*, 523. [CrossRef]
23. Fontes, C.J.; Colgan, J.; Zhang, H.L.; Abdallah, J., Jr. Large-scale kinetics modeling of non-LTE plasmas. *J. Quant. Spec. Rad. Transfer* **2006**, *99*, 175. [CrossRef]
24. Florido, R.; Rodríguez, R.; Gil, J.M.; Rubiano, J.G.; Mancini, R.C. Modelling of population kinetics of plasmas that are not in local thermodynamic equilibrium using a versatile collisional-radiative model. *Phys. Rev. E* **2009**, *80*, 056402. [CrossRef]

25. Fritzsche, S. Atomic input for modeling ionic mixtures in astrophysical plasma. *Eur. Phys. J. A* **2025**, *61*, 63. [CrossRef]
26. Forslund, D.W. Fundamentals of plasma simulation. *Space Sci. Rev.* **1985**, *42*, 3. [CrossRef]
27. Peratt, A.L. Advances in numerical modeling of astrophysical and space plasmas. *Astrophys. Space Sci.* **1996**, *242*, 93. [CrossRef]
28. Boyer, T.H. Blackbody radiation in classical physics: A historical perspective. *Am. J. Phys.* **2018**, *86*, 495. [CrossRef]
29. Raymond, J.C.; Cox, D.P.; Smith, B.W. Radiative cooling of a low-density plasma. *Astrophys. J.* **1976**, *204*, 290. [CrossRef]
30. Rybicki, G.B.; Lightman, A.P. *Radiative Processes in Astrophysics*; Wiley–VCH: New York, NY, USA, 1979.
31. Blumenthal, G.R.; Gould, R.J. Bremsstrahlung, synchrotron radiation, and Compton scattering of high-energy electrons traversing dilute gases. *Rev. Mod. Phys.* **1970**, *42*, 237. [CrossRef]
32. Chandrasekhar, S. *An Introduction to the Study of Stellar Structure*; University of Chicago Press: Chicago, IL, USA, 1939.
33. Fritzsche, S. RATIP—A toolbox for studying the properties of open-shell atoms and ions. *J. Electron Spectrosc. Relat. Phenom.* **2001**, *114–116*, 1155. [CrossRef]
34. Bethe, H.A.; Salpeter, E.E. *Quantum Mechanics of One- and Two-Electron Atoms*; Springer: Berlin, Germany, 1957.
35. Kramers, H.A. On the theory of X-ray absorption and of the continuous X-ray spectrum. *Phil. Mag.* **1923**, *46*, 836. [CrossRef]
36. Fierro, A.; Stephens, J.; Beeson, S.; Dickens, J.; Neuber, A. Discrete photon implementation for plasma simulations. *Phys. Plasmas* **2016**, *23*, 013506. [CrossRef]
37. Hillier, D.J. Photoionization and electron–ion recombination in astrophysical plasmas. *Atoms* **2023**, *11*, 54. [CrossRef]
38. Lihua, B.; Zeqing, W.; Bin, D.; Yongkun, D.; Jun, Y. Simulations of the spectrum from a photoionized Si plasma. *Phys. Plasmas* **2011**, *18*, 023301. [CrossRef]
39. Wadiak, E.J.; Sarazin, C.L.; Brown, R.L. Radio recombination lines from quasars. I. Level populations of hydrogenic ions in a strong, nonthermal radiation field. *Astrophys. J. Suppl.* **1983**, *53*, 351. [CrossRef]
40. Kodama, R. Stimulated free-bound emission from x-ray laser-interaction plasmas. *Phys. Rev. Lett.* **1992**, *69*, 77. [CrossRef] [PubMed]
41. Baig, M.A. Measurement of photoionization cross-section for the excited states of atoms: A review. *Atoms* **2022**, *10*, 39. [CrossRef]
42. Davis, J.; Clark, R.; Blaha, M.; Giuliani, J.L. Atomic physics and non-LTE effects. *Laser Part. Beams* **2001**, *19*, 557–577. [CrossRef]
43. Mashonkina, L.; Ryabchikova, T.; Ryabtsev, A.; Kildiyarova, R. Non-LTE line formation for Pr II and Pr III in A and Ap stars. *Astron. Astrophys.* **2009**, *495*, 297. [CrossRef]
44. Balakirev, V.A.; Karas, V.I.; Karas, I.V. Charged particle acceleration by an intense ultrashort electromagnetic pulse excited in a plasma by laser radiation or by relativistic electron bunches. *Plasma Phys. Rep.* **2002**, *28*, 125. [CrossRef]
45. Schippers, S.; Martins, M.; Beerwerth, R.; Bari, S.; Holste, K.; Schubert, K.; Viefhaus, J.; Savin, D.W.; Fritzsche, S.; Müller, A. Near L-edge single and multiple photoionization of singly charged iron ions. *Astrophys. J.* **2017**, *849*, 5. [CrossRef]
46. Beerwerth, R.; Buhr, T.; Perry-Sassmannshausen, A.; Stock, S.O.; Bari, S.; Holste, K.; Kilcoyne, A.L.D.; Reinwardt, S.; Ricz, S.; Savin, D.W.; et al. Near L-edge single and multiple photoionization of triply charged iron ions. *Astrophys. J.* **2019**, *887*, 189. [CrossRef]
47. Jacobs, V.L.; Behar, E.; Rozsnyai, B.F. Autoionization phenomena in dense photoionized plasmas. *J. Quant. Spectrosc. Radiat. Transf.* **2001**, *71*, 397. [CrossRef]
48. Perrot, F.; Dharma-Wardana, M.W.C. Equation of state and transport properties of an interacting multispecies plasma: Application to a multiply ionized Al plasma. *Phys. Rev. E* **1995**, *52*, 5352. [CrossRef]
49. Deprince, J.; Bautista, M.A.; Fritzsche, S.; García, J.A.; Kallman, T.R.; Mendoza, C.; Palmeri, P.; Quinet, P. Plasma environment effects on K lines of astrophysical interest. I. Atomic structure, radiative rates, and Auger widths of oxygen ions. *Astron. Astrophys.* **2019**, *624*, A74. [CrossRef]
50. Fritzsche, S.; Palmeri, P.; Schippers, S. Atomic cascade computations. *Symmetry* **2021**, *13*, 520. [CrossRef]
51. Fritzsche, S. Dielectronic recombination strengths and plasma rate coefficients of multiply charged ions. *Astron. Astrophys.* **2021**, *656*, A163. [CrossRef]
52. Fritzsche S. JAC: User Guide, Compendium & Theoretical Background. Unpublished (29.12.2025), Version v0.3.0. Available online: <https://github.com/OpenJAC/JAC.jl> (accessed on 10 December 2025).
53. Oelgoetz, J.; Pradhan, A.K. The 6.7-keV $K\alpha$ complex of He-like iron in transient plasmas. *Mon. Not. R. Astron. Soc.* **2004**, *354*, 1093. [CrossRef]
54. Gnat, O. Time-dependent cooling in photoionized plasma. *Astrophys. J. Suppl. Ser.* **2017**, *228*, 11. [CrossRef]

Disclaimer/Publisher’s Note: The statements, opinions and data contained in all publications are solely those of the individual author(s) and contributor(s) and not of MDPI and/or the editor(s). MDPI and/or the editor(s) disclaim responsibility for any injury to people or property resulting from any ideas, methods, instructions or products referred to in the content.